Inorganic Chemistry

Article

pubs.acs.org/IC

Tetraanionic Biphenyl Lanthanide Complexes as Single-Molecule Magnets

Wenliang Huang,[†,‡,∥] Jennifer J. Le Roy,[§,∥] Saeed I. Khan,[†] Liviu Ungur,*[,⊥] Muralee Murugesu,*[,§] and Paula L. Diaconescu*[,†]

[†]Department of Chemistry and Biochemistry, University of California, Los Angeles, California 90095, United States

[§]Department of Chemistry, University of Ottawa, Ottawa, Ontario KIN 6N5, Canada

[⊥]Theory of Nanomaterials Group and INPAC Institute for Nanoscale Physics and Chemistry, Katholieke Universiteit Leuven, Celestijnenlaan, 200F 3001, Belgium

Supporting Information

ABSTRACT: Inverse sandwich biphenyl complexes $[(NN^{TBS})Ln]_2(\mu$-biphenyl$)[K(solvent)]_2$ [NN^{TBS} = 1,1′-fc(NSi^{t}BuMe$_2$)$_2$; Ln = Gd, Dy, Er; solvent = Et_2O, toluene; 18-crown-6], containing a quadruply reduced biphenyl ligand, were synthesized and their magnetic properties measured. One of the dysprosium biphenyl complexes was found to exhibit antiferromagnetic coupling and single-molecule-magnet behavior with U_{eff} of 34 K under zero applied field. The solvent coordinated to potassium affected drastically the nature of the magnetic interaction, with the other dysprosium complex showing ferromagnetic coupling. Ab initio calculations were performed to understand the nature of magnetic coupling between the two lanthanide ions bridged by the anionic arene ligand and the origin of single-molecule-magnet behavior.

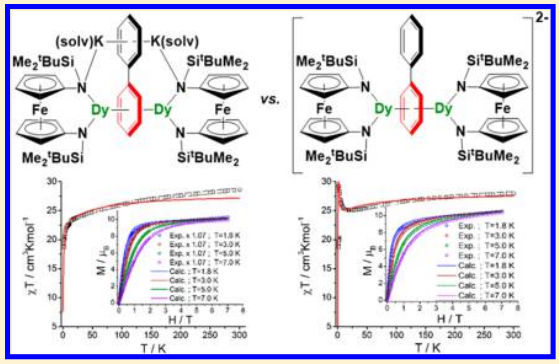

INTRODUCTION

Lanthanide single-molecule magnets (SMMs) show fast improvement upon an increase in the anisotropic barrier and/or a rise in the blocking temperature limit to exhibit magnetic hysteresis.[1−3] Because of the complexity of the 4f shell, it is difficult to elucidate the electronic structure of paramagnetic lanthanide complexes, especially of those usually employed in SMMs, i.e., dysprosium and terbium.[4] Several methods have been proposed for predicting the anisotropic barriers of various lanthanide compounds with an emphasis on either a high- or low-symmetry coordination environment.[4,5] Despite these efforts, the factors governing a large magnetic anisotropy are beyond simple models, especially in molecules containing more than one 4f ion. A noticeable case is $[([(Me_3Si)_2N]_2(THF)Tb)_2(\mu$-$N_2)]^-$,[6] which exhibits magnetic hysteresis at a relatively high temperature (14 K) compared to other examples.[1−3] The strong exchange coupling induced by the bridging N_2^{3-} radical trianion was proposed to be responsible for the magnetic properties of this complex.[7] It is interesting to note that, for actinides, an arene-bridged diuranium complex has shown SMM behavior.[8] However, structurally analogous arene-bridged lanthanide complexes have not been available until recently and, therefore, their magnetic properties could not be studied. Our group reported the synthesis of inverse sandwiches of a biphenyl, $[(NN^{TBS})Ln]_2(\mu$-biphenyl$)[K(solvent)]_2$ [NN^{TBS} = 1,1′-fc(NSi^{t}BuMe$_2$)$_2$; Ln = Sc, Y, La, Lu; solvent = Et_2O, toluene, THF, 18-crown-6],[9] containing a quadruply reduced biphenyl ligand and the metal ions coordinated to the same phenyl ring.

Experimental and computational studies indicated that the quadruply reduced biphenyl in $[(NN^{TBS})Ln]_2(\mu$-biphenyl$)[K(solvent)]_2$ has the charge localized on the phenyl ring coordinated to the two rare earths. The overall molecule is stabilized by δ-symmetry overlap between two π^* orbitals of the phenyl ring and metal-based orbitals. This electronic structure similar to that of diuranium arene complexes[8,10−18] prompted us to explore the properties of the corresponding paramagnetic lanthanides, $[(NN^{TBS})Ln]_2(\mu$-biphenyl$)[K(solvent)]_2$ (**Ln_2-biph**, where Ln = Dy, Gd, and Er). More specifically, we focused our attention toward the highly anisotropic Kramers ions dysprosium and erbium and the isotropic gadolinium analogue. The gadolinium compound provided an avenue to probe the nature and strength of the interaction between the metal centers. Herein, we report the synthesis and characterization of dysprosium, gadolinium, and erbium biphenyl complexes and a study of the magnetic properties of those complexes.

EXPERIMENTAL SECTION

General Considerations. All experiments were performed under a dry nitrogen atmosphere using standard Schlenk techniques or an MBraun inert-gas glovebox unless otherwise specified. Solvents

Received: December 15, 2014
Published: February 19, 2015

DOI: 10.1021/ic5029788
Inorg. Chem. 2015, 54, 2374−2382

toluene, hexanes, diethyl ether (Et_2O), and tetrahydrofuran (THF) were purified using a two-column solid-state purification system by the method of Grubbs[19] and transferred to the glovebox without exposure to air. *n*-Pentane was distilled over calcium hydride under a dinitrogen atmosphere. Methanol was distilled over calcium oxide under a dinitrogen atmosphere. All solvents were stored on activated molecular sieves and/or sodium for at least a day prior to use. NMR solvents benzene-d_6 (C_6D_6) and THF-d_8 (C_4D_8O) were obtained from Cambridge Isotope Laboratories, degassed or brought directly into a glovebox in a sealed ampule, and stored over activated molecular sieves for one week prior to use. Biphenyl was purchased from Sigma-Aldrich and used as received. 18-Crown-6 was purchased from Alfa-Aesar and crystallized from hexanes after passing through an alumina plug. Benzylpotassium (KBn),[20] $H_2(NN^{TBS})$ [NN^{TBS} = 1,1′-fc-(NSi^tBuMe_2)$_2$],[21] (NN^{TBS})GdI(THF)$_2$, and (NN^{TBS})ErI(THF)$_2$[22] were prepared following literature protocols. NMR spectra were recorded on Bruker AV300, Bruker DRX500, Bruker AV500 (work supported by NSF Grant CHE-1048804), and Bruker AV600 spectrometers at 25 °C in C_6D_6 or C_4D_8O unless otherwise specified. Chemical shifts are reported with respect to the internal solvent (C_6D_6 at 7.16 ppm or C_4D_8O at 1.73 ppm). CHN analyses were performed in house on a CE-440 elemental analyzer manufactured by Exeter Analytical, Inc.

Magnetic Measurements. Magnetic susceptibility measurements for all complexes were obtained using a Quantum Design SQUID magnetometer MPMS-XL7 operating between 1.8 and 300 K for direct-current (dc) applied fields ranging from −7 to +7 T. dc analyses were performed on polycrystalline samples sealed in a polyethylene membrane (prepared in an inert atmosphere) under a field ranging from 0 to 7 T and temperatures between 1.8 and 300 K. Alterating-current (ac) susceptibility measurements were carried out under an oscillating ac field of 3 Oe and ac frequencies ranging from 1 to 1500 Hz. Magnetization data were collected at 100 K to check for ferromagnetic impurities that were absent in all samples. In addition, data were collected on different batches to check for consistency. Diamagnetic corrections were applied for the sample holder and the core diamagnetism from the sample (estimated with Pascal constants).

Ab Initio Calculations. All calculations on individual magnetic centers were done with *MOLCAS 7.8* and are of the CASSCF/RASSI/SINGLE_ANISO type. For Dy^{3+}, the active space of the CASSCF included nine electrons in seven 4f orbitals. The spin−orbit coupling included the mixing of 21 sextets, 128 quartets, and 130 doublet states. For Er^{3+}, the active space of the CASSCF included 11 electrons in seven 4f orbitals. The spin−orbit coupling included the mixing of 35 spin quartets and 112 spin doublet states. Two structures were employed: a complete structure and a reduced structure. In the reduced structure, all methyl and *tert*-butyl groups were replaced by hydrogen. Three basis sets were employed [MB (minimal), DZP (medium), and TZP (large)].

Synthesis of $DyBr_3(THF)_{3.5}$. $DyBr_3(THF)_{3.5}$ was synthesized following a protocol similar to that for $GdBr_3(THF)_{3.5}$.[22] In a 1 L three-neck round-bottomed flask, Dy_2O_3 (9.325 g, 25 mmol) and NH_4Br (20.060 g, 205 mmol) were added, followed by the addition of 120 mL of concentrated hydrobromic acid (48%, w/w aqueous). The mixture was heated under a constant air flow to remove H_2O and HBr (which is absorbed by a 10% sodium hydroxide solution). After ca. 12 h, the resulting white solid was transferred into a sublimation tube. The solid was heated under vacuum to remove water (140 °C for a minimum of 8 h) to form $(NH_4)_3(DyBr_6)$ (250 °C for 8 h) and eventually to dehydrate $DyBr_3$.[23] After cooling to room temperature, the sublimation tube was brought into a glovebox and the fluffy off-white solid of $DyBr_3$ (360 °C for 8 h) was separated from the rocklike NH_4Br crystals (which were located on the upper part of the tube). Yield for $DyBr_3$: 15.984 g, 79.5%. Solid $DyBr_3$ was then transferred into a 350 mL Schlenk tube, and 50 mL of THF was carefully added (the reaction is highly exothermic and may result in boiling and even decomposition of THF to form carbon black). The white suspension was heated at 50 °C for 2 h. The volatiles were removed under reduced pressure to give an off-white microcrystalline solid. Yield for $DyBr_3(THF)_{3.5}$: 25.219 g, 96.9%. Overall yield from Dy_2O_3: 77.0%. The empirical formula $DyBr_3(THF)_{3.5}$ was determined by considering the mass change upon treatment with THF[22] and used as such in subsequent procedures.

Synthesis of (NN^{TBS})DyI(THF)$_2$. (NN^{TBS})DyI(THF)$_2$ was synthesized following a protocol similar to that for (NN^{TBS})GdI(THF)$_2$.[22] In a 100 mL round-bottomed flask were added $DyBr_3(THF)_{3.5}$ (1.0000 g, 1.528 mmol) and 60 mL of THF. The suspension was chilled with a dry ice/acetone bath for 15 min. In a 20 mL scintillation vial were added KBn (0.5970 g, 4.584 mmol) and 15 mL of THF to give a red solution, which was chilled with a dry ice/acetone bath for 10 min. The KBn solution was added dropwise to the $DyBr_3$ suspension with stirring and constant chilling by a dry ice/acetone bath. Shortly after the addition, the red color of KBn disappeared, and the resulting gray suspension was allowed to stir at 0 °C (ice bath) for 30 min. The suspension was then filtered through Celite and washed with ca. 10 mL of THF. The washings were combined with the filtrate and transferred to a clean 100 mL round-bottomed flask (ca. 70 mL). The gray solution (in situ formed $DyBn_3(THF)_3$) was chilled with a dry ice/acetone bath for 15 min. In a 20 mL scintillation vial were added $H_2(NN^{TBS})$ (0.6790 g, 1.527 mmol) and 10 mL of THF. The vial was chilled with a dry ice/acetone bath for 10 min. A $H_2(NN^{TBS})$ solution was added dropwise to the $DyBn_3(THF)_3$ solution with stirring and constant chilling with a dry ice/acetone bath. After the addition, the solution color turned to orange. The solution was stirred at 0 °C (ice bath) for 1 h before removal of the volatiles. After removal of the volatiles, the resulted orange solid was extracted into ca. 20 mL of toluene and filtered through Celite to remove any remaining insoluble impurities. To the orange solution [in situ formed (NN^{TBS})DyBn(THF)] was added 2 mL of a toluene solution of Me_3SiI (0.6110 g, 3.054 mmol) at 25 °C. The solution was allowed to stir at 25 °C for 1 h. Then ca. 2 mL of THF was added to quench the excess Me_3SiI, and the volatiles were removed under reduced pressure to yield an orange solid. Crystallization from a minimum amount of Et_2O (ca. 20 mL) layered with *n*-pentane (ca. 20 mL) at −35 °C yielded orange crystals of (NN^{TBS})DyI(THF)$_2$. Yield: first crop of 0.7104 g, 52.7%. The mother liquor was concentrated to yield a second crop of 0.205 g, 15.5%. Total yield: 68.2%. Single crystals of (NN^{TBS})DyI(THF)$_2$ were grown from an Et_2O solution layered with *n*-pentane. Anal. Calcd for $C_{30}H_{54}N_2O_2FeDySi_2I$ with one molecule of *n*-pentane (C_5H_{12}; M_w = 948.346): C, 44.32; H, 7.02; N, 2.95. Found: C, 44.26; H, 6.94; N, 2.96.

Synthesis of Dy_2-biph. **Dy_2-biph** was synthesized following a protocol similar to that for **Y_2-biph**.[9] In a 20 mL scintillation vial, (NN^{TBS})DyI(THF)$_2$ (0.4000 g, 0.457 mmol) and biphenyl (0.0352 g, 0.228 mmol) were dissolved in ca. 10 mL of THF. The vial was chilled with a dry ice/acetone bath for 10 min. KC_8 (0.1543 g, 1.141 mmol) was added to the THF solution. The mixture was warmed up to 25 °C and allowed to stir for 10 min before filtering through Celite to remove the byproducts, graphite, and potassium iodide. The volatiles were removed under reduced pressure to yield a black solid. The solid was washed with ca. 15 mL of Et_2O, and a microcrystalline black solid of **Dy_2-biph** was collected on a medium frit. Yield: 0.2550 g, 70.2%. **Dy_2-biph** synthesized as such has a formula of [(NN^{TBS})Dy]$_2$(μ-biphenyl)[K(OEt_2)]$_2$. Single crystals of **Dy_2-biph** were grown from a toluene solution layered with hexanes with a formula of [(NN^{TBS})Dy]$_2$(μ-biphenyl)[K(toluene)]$_2$. Anal. Calcd for $C_{64}H_{106}N_4O_2Fe_2Dy_2Si_4K_2$ (with one Et_2O as a coordinating solvent for each potassium; M_w = 1590.808): C, 48.32; H, 6.72; N, 3.52. Found: C, 48.06; H, 6.76; N, 3.85.

Synthesis of Dy_2-biph-crown$_2$. **Dy_2-biph** (0.0949 g, 0.0597 mmol) and 2 equiv of 18-crown-6 (0.0315 g, 0.119 mmol) were weighed in a 20 mL scintillation vial. Cold THF (5 mL) was added, and the mixture was allowed to stir at −78 °C for 1 h. Volatiles were removed under reduced pressure, and the resulting solid was washed with Et_2O. The black solid was then dissolved in THF and the solution layered with *n*-pentane. Black crystals formed after the solution was stored in a −35 °C freezer for 1 day. Yield: 0.1182 g, 93.5%. Single crystals of **Dy_2-biph-crown$_2$** were grown from a THF solution layered with *n*-pentane. Anal. Calcd for $C_{88}H_{150}N_4O_{14}Fe_2Dy_2Si_4K_2$ (with one THF molecule coordinated to potassium in addition to 18-crown-6;

DOI: 10.1021/ic5029788
Inorg. Chem. 2015, 54, 2374−2382

M_w = 2115.414): C, 49.97; H, 7.15; N, 2.65. Found: C, 49.33; H, 6.98; N, 2.70.

Synthesis of Gd_2-biph. **Gd_2-biph** was synthesized following a protocol similar to that for **Dy_2-biph**. Scale: $(NN^{TBS})GdI(THF)_2$ (0.3000 g, 0.344 mmol), biphenyl (0.0266 g, 0.172 mmol), and KC_8 (0.1164 g, 0.861 mmol). Yield: 0.1950 g, 71.6%. **Gd_2-biph** synthesized as such has a formula of $[(NN^{TBS})Gd]_2(\mu\text{-biphenyl})[K(OEt_2)]_2$. Single crystals of **$Dy_2$-biph** were grown from a toluene solution layered with hexanes with a formula of $[(NN^{TBS})Gd]_2(\mu\text{-biphenyl})[K(toluene)]_2$. Anal. Calcd for $C_{64}H_{106}N_4O_2Fe_2Gd_2Si_4K_2$ (with one Et_2O as a coordinating solvent for potassium; M_w = 1580.308): C, 48.64; H, 6.76; N, 3.54. Found: C, 48.38; H, 6.63; N, 3.47.

Synthesis of Gd_2-biph-crown$_2$. **Gd_2-biph** (0.1345 g, 0.0851 mmol) and 2 equiv of 18-crown-6 (0.0440 g, 0.166 mmol) were weighed in a scintillation vial. Cold THF (5 mL) was added, and the mixture was allowed to stir at −78 °C for 1 h. Volatiles were removed under reduced pressure, and the resulting solid was washed with Et_2O. The black solid was then dissolved in THF and the solution layered with *n*-pentane. Black crystals formed after the solution was stored in a −35 °C freezer for 1 day. Yield: 0.1200 g, 67.0%. Single crystals of **Dy_2-biph-crown$_2$** were grown from a THF solution layered with *n*-pentane. Anal. Calcd for $C_{88}H_{150}N_4O_{14}Fe_2Gd_2Si_4K_2$ (with one THF molecule coordinated to potassium in addition to 18-crown-6; M_w = 2104.914): C, 50.23; H, 7.19; N, 2.66. Found: C, 50.31; H, 7.27; N, 2.78.

Synthesis of Er_2-biph. **Er_2-biph** was synthesized following a protocol similar to that for **Dy_2-biph**. Scale: $(NN^{TBS})ErI(THF)_2$ (0.4000 g, 0.454 mmol), biphenyl (0.0350 g, 0.227 mmol), and KC_8 (0.1535 g, 1.135 mmol). Yield: 0.2413 g, 66.4%. **Er_2-biph** synthesized as such has a formula of $[(NN^{TBS})Er]_2(\mu\text{-biphenyl})[K(OEt_2)]_2$. Single crystals of **$Er_2$-biph** were grown from an Et_2O solution. Anal. Calcd for $C_{64}H_{106}N_4O_2Fe_2Er_2Si_4K_2$ (with one Et_2O as a coordinating solvent for potassium) and one extra Et_2O molecule (M_w = 1674.451): C, 48.77; H, 6.98; N, 3.35. Found: C, 49.49; H, 6.28; N, 3.50.

Synthesis of Er_2-biph-crown$_2$. **Er_2-biph** (0.1045 g, 0.0653 mmol) and 2 equiv of 18-crown-6 (0.0345 g, 0.131 mmol) were weighed in a 20 mL scinillation vial. Cold THF (5 mL) was added, and the mixture was allowed to stir at −78 °C for 1 h. Volatiles were removed under reduced pressure, and the resulting solid was washed with Et_2O. The black solid was then dissolved in THF and the solution layered with *n*-pentane. Black crystals formed after the solution was stored in a −35 °C freezer for 1 day. Yield: 0.1307 g, 95.2%. Single crystals of **Er_2-biph-crown$_2$** were grown from a THF solution layered with *n*-pentane. Anal. Calcd for $C_{88}H_{150}N_4O_{14}Fe_2Er_2Si_4K_2$ (with one THF molecule coordinated to potassium in addition to 18-crown-6) and 1.5 molecules of hexanes (C_6H_{14}; M_w = 2326.306): C, 52.15; H, 7.76; N, 2.41. Found: C, 52.60; H, 7.13; N, 2.55.

RESULTS AND DISCUSSION

Synthesis and Characterization of Tetraanionic Biphenyl Lanthanide Complexes. The metal precursors $(NN^{TBS})LnI(THF)_2$ (**LnI**, where Ln = Dy, Gd, and Er) can be synthesized following a protocol similar to that developed for other paramagnetic lanthanides.[22] Compounds **Gd_2-biph**, **Dy_2-biph**, and **Er_2-biph** could be isolated in high yield analogously to **Y_2-biph** (Scheme 1a).[9] Similar to **Y_2-biph**, the separated ion-pair version, $([(NN^{TBS})Ln]_2(\mu\text{-biphenyl}))[K(18\text{-crown-6})(THF)_{1.5}]_2$ (**Ln_2-biph-crown$_2$**, where Ln = Dy, Gd, and Er), could also be synthesized by treating **Ln_2-biph** with 2 equiv of 18-crown-6, followed by crystallization from THF/*n*-pentane (Scheme 1b).

The molecular structures of **Ln_2-biph** and **Ln_2-biph-crown$_2$** (Ln = Dy, Gd, Er) were determined by X-ray crystallography; those of **Dy_2-biph** and **Dy_2-biph-crown$_2$** are shown in Figure 1 as representative examples. Crystallized from a toluene solution layered with hexanes, **Dy_2-biph** and **Gd_2-biph** are isostructural to **Y_2-biph** with a toluene molecule as the coordinating solvent

Scheme 1. (a) Synthesis of Ln_2-biph and (b) Ln_2-biph-crown$_2$ (Ln = Gd, Dy, Er)

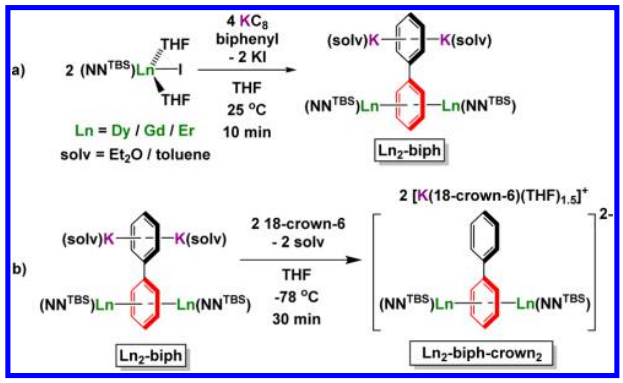

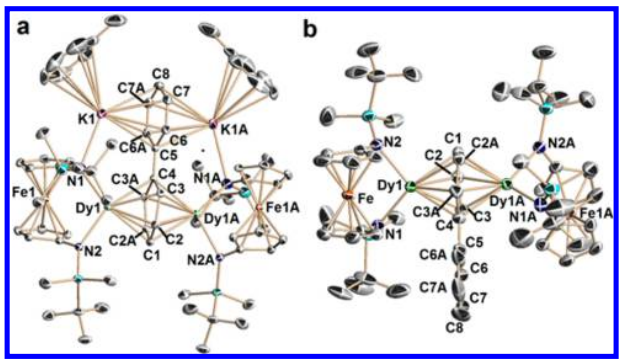

Figure 1. Molecular structures of (a) **Dy_2-biph-toluene** and (b) **Dy_2-biph-crown$_2$** with thermal ellipsoids drawn at the 50% probability level. Hydrogen atoms and disordered counterparts were omitted for clarity.

for K^+. However, **Er_2-biph**, which is crystallized from a Et_2O solution, has Et_2O as a coordinating solvent for K^+. Despite the difference in the coordinating solvent for K^+, the coordination environment around each lanthanide ion is similar in all **Ln_2-biph**.

Table 1 summarizes some informative structural parameters for **Ln_2-biph** and **Ln_2-biph-crown$_2$**. The average Ln−N, Ln−C, and Ln−Ln distances follow the general trend of the ionic radii of metal ions. The Ln−Ln distances are rather short at 4.268(1), 4.194(1), and 4.138(1) Å for Gd, Dy, and Er, respectively, for **Ln_2-biph**. The Dy−Dy distance is comparable to the Dy−Dy distance of 4.14 Å in the triple-decker complex $Dy_2(COT'')_3$ [COT'' = 1,4-bis(trimethylsilyl)-cyclooctatetraenyl dianion, 1,4-$(SiMe_3)_2$-COT].[24]

The Ln−C and Ln−Ln distances are even shorter in the separated ion-pair complexes **Ln_2-biph-crown$_2$**. For example, the average Dy−C and Dy−Dy distances in **Dy_2-biph-crown$_2$** are 2.525(7) and 4.107(2) Å, respectively, 0.03 and 0.08 Å shorter than the corresponding parameters of **Dy_2-biph**. Together with the longer average C−C distance found for the phenyl ring coordinated to the lanthanides, these structural features reflect a stronger metal−arene interaction and a more localized charge on the coordinating phenyl ring upon exclusion of potassium.

In the previous **Ln_2-biph** series (Ln = Sc, Y, Lu), we noticed the following trend in the torsion angle (defined by the dihedral angles C2−C3−C3A−C2A and C3−C2−C2A−C3A in Figure 1a and indicating the degree of distortion from planarity) of the

DOI: 10.1021/ic5029788
Inorg. Chem. 2015, 54, 2374−2382

Table 1. Structural Parameters for Ln_2-biph (Ln1 in Table, Where Ln = Gd, Dy, and Er) and Ln_2-biph-crown$_2$ (Ln2 in Table, Where Ln = Gd, Dy, and Er) (Distances in Angstroms and Angles in Degrees)

	Gd1	Gd2	Dy1	Dy2	Er1	Er2
R(Ln)[a]	1.08	1.08	1.05	1.05	1.03	1.03
Ln−Ln	4.27	4.22	4.19	4.11	4.14	4.07
Ln−Fe	3.20	3.25	3.21	3.26	3.23	3.26
Ln−N[b]	2.37	2.38	2.33	2.33	2.31	2.31
Ln−C[b,c]	2.58	2.57	2.55	2.53	2.53	2.51
C−C[d]	1.46	1.46	1.46	1.47	1.46	1.47
C_{ipso}−C_{ipso}	1.41	1.46	1.41	1.42	1.42	1.44
torsion[e]	10	12	−11	−11	−14	−14
dihedral[f]	−162	−136	161	127	145	126

[a]From ref 25. [b]Average value for the Ln−N and Ln−C distances. [c]Carbon atoms of the coordinated phenyl ring. [d]Average C−C distance in the coordinated phenyl ring. [e]Torsion angle defined by the average of the dihedral angles C_{meta}−C_{ortho}−C_{ortho}−C_{meta} and C_{ortho}−C_{meta}−C_{meta}−C_{ortho} of the coordinated phenyl ring. [f]Dihedral angle Fe−Ln−Ln−Fe.

coordinated phenyl ring: the smaller the metal ions, the larger the torsion angle. This trend is also observed for **Gd_2-biph**, **Dy_2-biph**, and **Er_2-biph**. In addition, the dihedral angle Fe−Ln−Ln−Fe (Fe1−Dy1−Dy1A−Fe1A in Figure 1a) is a measure of the relative position of the two lanthanide units. Upon the removal of K^+ by 18-crown-6, a significant decrease of that angle was observed for all lanthanides (Gd, 26°; Dy, 34°; Er, 19°).

Magnetism of Tetraanionic Biphenyl Lanthanide Complexes. Solid-state magnetic properties of all six complexes were investigated using a superconducting quantum interference device (SQUID). Analyses were performed on crushed polycrystalline samples sealed in a polyethylene membrane prepared and sealed under an inert atmosphere. dc susceptibility measurements were carried out under a 0.1 T applied dc field over the temperature range of 1.8−300 K (Figure 2). The room temperature χT values of 28.59 cm^3 K mol^{-1} (**Dy_2-biph**) and 27.95 cm^3 K mol^{-1} (**Dy_2-biph-crown$_2$**) are in good agreement with the theoretical value of 28.34 cm^3 K mol^{-1} for two noninteracting dysprosium(III) ions ($^6H_{15/2}$, $S = {}^5/_2$, $L = 5$, $g_J = {}^4/_3$). Similarly, the room temperature χT values of 21.87 cm^3 K mol^{-1} (**Er_2-biph**) and 22.59 cm^3 K mol^{-1} (**Er_2-biph-crown$_2$**) are in good agreement with the theoretical value of 22.96 cm^3 K mol^{-1} for two noninteracting erbium(III) ions ($^4I_{15/2}$, $S = {}^3/_2$, $L = 6$, $g_J = {}^6/_5$). Lastly, for **Gd_2-biph** and **Gd_2-biph-crown$_2$**, the respective room temperature χT values of 15.63 and 15.83 cm^3 K mol^{-1} are in good agreement with the theoretical value of 15.76 cm^3 K mol^{-1} for two noninteracting gadolinium(III) ions ($^8S_{7/2}$, $S = {}^7/_2$, $L = 0$, $g_J = 2$).

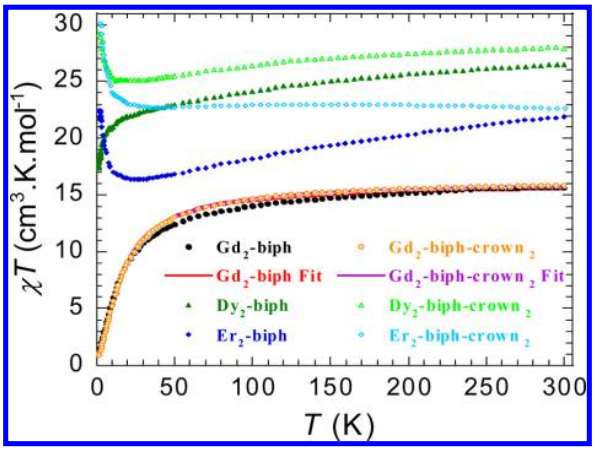

Figure 2. Temperature dependence of the χT product at 0.1 T for **Gd_2-biph** (●), **Gd_2-biph-crown$_2$** (○), **Dy_2-biph** (▲), **Dy_2-biph-crown$_2$** (△), **Er_2-biph** (◆), and **Er_2-biph-crown$_2$** (◇), with χ being the molar susceptibility per molecule defined as M/H.

The χT product of **Dy_2-biph** decreases gradually from 300 K with decreasing temperature with a steep decrease below 20 K to reach a minimum value of 18.73 cm^3 K mol^{-1} at 1.8 K. The low-temperature decrease may be attributed to several factors including significant anisotropy inherent to dysprosium(III) ions as well as an antiferromagnetic interaction between dysprosium centers. The χT product of **Dy_2-biph-crown$_2$** shows behavior similar to that of **Dy_2-biph** from 300 to 20 K; however, interestingly, below 20 K, there is a sharp increase to reach a maximum value of 29.19 cm^3 K mol^{-1} at 1.8 K, indicating the presence of dominant ferromagnetic interactions between the spin carriers. This interaction is likely intramolecular in nature because the closest intermolecular Dy−Dy distance is 14.25 Å. This remarkable change in the magnetic properties due to the secondary coordination environment is in agreement with recently reported results, showing that the overall properties of lanthanide SMMs can be altered by small structural modifications.[26]

The variable-temperature χT plots of the two erbium complexes resemble the data for **Dy_2-biph-crown$_2$**. A slight decrease of the χT product was observed up to 20 K followed by a sharp increase, reaching maximum values of 21.87 cm^3 K mol^{-1} for **Er_2-biph** and 30.06 cm^3 K mol^{-1} for **Er_2-biph-crown$_2$** at 1.8 K. Such behavior indicates again ferromagnetic interactions between the two erbium ions in both complexes. Because the dysprosium and erbium systems are highly anisotropic, employment of Kambe's coupling method to obtain the coupling strength is not valid; thus, we focused our efforts in attaining coupling strength in the isotropic gadolinium analogues. For **Gd_2-biph** and **Gd_2-biph-crown$_2$**, the χT product remains fairly linear with decreasing temperature, with a sharp decrease below 50 K to reach minimum values at 1.8 K of 1.17 and 0.94 cm^3 K mol^{-1}, respectively. In both **Gd_2-biph** and **Gd_2-biph-crown$_2$**, this low-temperature decrease is primarily caused by antiferromagnetic coupling between isotropic gadolinium ions.

In order to quantify the strength of the Gd−Gd interaction in both complexes, application of the Van Vleck equation to Kambe's vector coupling method was employed using the isotropic spin Hamiltonian $H = -2JS_a \cdot S_b$ with $S_a = S_b = {}^7/_2$, which was used to fit variation of the χT versus T data. The

DOI: 10.1021/ic5029788
Inorg. Chem. 2015, 54, 2374−2382

best-fit parameters obtained are $J = -0.642(6)$ cm^{-1}, $g = 2.01(7)$ and $J = -0.664(6)$ cm^{-1}, $g = 2.03(7)$ for **Gd_2-biph** and **Gd_2-biph-crown$_2$**, respectively. Although relatively weak, the Gd−Gd coupling in both complexes surprisingly shows an increase in J over the COT-bridged Gd^{III}_2 complex[24] [$J = -0.447(7)$ cm^{-1}] despite a similar Ln−Ln separation. This suggests that, in the present arene-bridged system, the Ln−C_{biph} interaction is stronger than Ln−C_{COT}, which is likely a consequence of the significant metal−phenyl orbital overlap, as shown by density functional theory (DFT) calculations on the diamagnetic counterpart, **Y_2-biph**.[9] The slight difference in J between **Gd_2-biph** and **Gd_2-biph-crown$_2$** is consistent with a decreasing Gd−Gd distance. A difference in the magnetic coupling (ferromagnetic vs antiferromagnetic) of different lanthanide analogues, such as that observed in **Dy_2-biph-crown$_2$**, **Er_2-biph-crown$_2$**, and **Gd_2-biph-crown$_2$**, has been previously reported by Ishikawa et al.[27] However, when considering all six complexes, it is interesting that ferromagnetic interactions are observed in complexes with closer Ln−Ln distances (4.14 Å or less) and antiferromagnetic interactions are observed in **Dy_2-biph**, **Gd_2-biph-crown$_2$**, and **Gd_2-biph**, each having Ln−Ln distances greater than 4.14 Å.

In order to determine the presence of magnetic anisotropy, field-dependent magnetization measurements were performed on all six complexes between 1.8 and 7 K at fields ranging from 0 to 7 T (Figures S8−S13 in the Supporting Information, SI). In **Dy_2-biph** and **Dy_2-biph-crown$_2$**, the magnetization data below 7 K revealed a rapid increase in magnetization at low magnetic fields with a more gradual increase above 2 T, reaching near-saturation at low temperatures [$M = 9.62(6)$ μ_B at 1.8 K under 7 T (**Dy_2-biph**); $M = 10.5(1)$ μ_B at 1.8 K under 7 T (**Dy_2-biph-crown$_2$**)]. Both nonsaturation in the M versus H data as well as nonsuperimposition of isotemperature lines in the M versus H/T plot suggests nonnegligible magnetic anisotropy in both complexes (Figures S8 and S9 in the SI). Both **Er_2-biph** and **Er_2-biph-crown$_2$** exhibit near-identical magnetization and reduced magnetization behavior with their respective dysprosium analogues; hence, magnetic anisotropy is also present in these complexes. Near-saturation at 1.8 K is observed in the magnetization data of **Er_2-biph**, with $M = 7.77(4)$ μ_B, and **Er_2-biph-crown$_2$**, with $M = 7.74(5)$ μ_B under 7 T. In contrast to the dysprosium and erbium complexes, the reduced magnetization measurements performed on **Gd_2-biph** and **Gd_2-biph-crown$_2$** reveal a linear relationship, as expected for antiferromagnetically coupled isotropic spin carriers. Because of the dominant antiferromagnetic coupling at low temperatures, the spin ground state for the gadolinium analogue is expected to be a singlet. Therefore, the observed linear curves are likely due to the presence of low-lying excited states that are thermally accessible. The isotropic nature of gadolinium precludes the possibility of SMM behavior in **Gd_2-biph** and **Gd_2-biph-crown$_2$** complexes.

In order to investigate the magnetic relaxation dynamics of the dysprosium and erbium complexes, ac magnetic susceptibility measurements were performed. For **Dy_2-biph**, under zero applied dc field, a strong temperature- and frequency-dependent χ'' signal was observed. Temperature-dependent χ'' data revealed full frequency-dependent peaks with peak maxima shifting toward lower temperatures between 9 and 4.5 K, consistent with SMM behavior (Figure S14 in the SI). Below 4.5 K, frequency-independent peaks are observed, indicating quantum tunneling of magnetization (QTM) at low temperature.

The anisotropic barrier, $U_{eff} = 34$ K, $\tau_0 = 1.6 \times 10^{-6}$ s, was determined by using an Arrhenius equation [$\tau = \tau_0 \exp(U_{eff}/kT)$]. This barrier is relatively small compared to those of other didysprosium SMMs[2] but is comparable to that for the aromatic COT′′-bridged complex, $Dy_2(COT'')_3$ ($U_{eff} = 25$ K, $\tau_0 = 1.6 \times 10^{-6}$ s).[24] This relatively small barrier is attributed to the presence of significant QTM observed in the χ'' data (Figure S14 in the SI). Upon application of an optimum static dc field of 900 Oe, QTM was reduced in **Dy_2-biph** (Figures 3

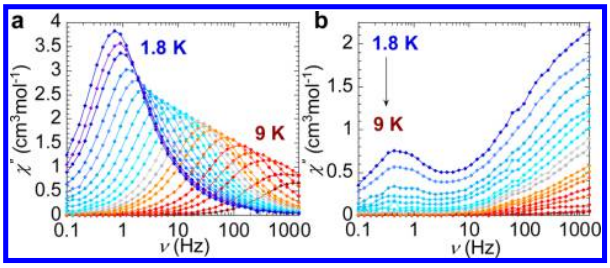

Figure 3. Out-of-phase (χ'') ac magnetic susceptibility for **Dy_2-biph** (a) and **Dy_2-biph-crown$_2$** (b) from 1.8−9 K under an applied dc field of 900 Oe.

and S15 in the SI). As expected, a decrease of the frequency-independent peak maxima in the χ'' data below 4.5 K (Figure 3) as well as a significant improvement in the anisotropic barrier, $U_{eff} = 53$ K, $\tau_0 = 1.5 \times 10^{-7}$ s (Figure S16 in the SI), was observed. The antiferromagnetic Dy−Dy interaction (determined from the χT data) implies that this energy barrier originates from a single-ion effect, as observed in the previously reported $Dy_2(COT'')_3$ complexes.[24]

The ac magnetic susceptibility of **Dy_2-biph-crown$_2$** was radically different from that of **Dy_2-biph**: surprisingly, no ac signal was observed under zero applied dc field. However, under a 900 Oe applied dc field, frequency-dependent studies reveal a peak at low frequency and an additional tail at high frequency at 1.8 K (Figures 3 and S17 in the SI). The observed peak is frequency-independent with varying temperature and, therefore, signifies a significant QTM relaxation process. Surprisingly, even under an applied dc field, no clear blocking of the magnetization was observed in **Dy_2-biph-crown$_2$**; therefore, no energy barrier could be extracted for this complex. As mentioned previously, it has been recently demonstrated that even small changes in the secondary coordination sphere can have a large impact on the magnetic anisotropy axis of lanthanide(III) ions.[24,26] The decrease in the magnetic performance of **Dy_2-biph-crown$_2$** compared to **Dy_2-biph** is unexpected because of the ferromagnetic interaction between dysprosium ions in **Dy_2-biph-crown$_2$** and the antiferromagnetic interaction in **Dy_2-biph**. These results are additionally surprising when the smaller coordination environment around each dysprosium ion in **Dy_2-biph** compared to **Dy_2-biph-crown$_2$** is considered. A small coordination environment in such low-symmetry complexes can quench the orbital angular momentum because of increased electron repulsion; therefore, the stronger magnetic performance of **Dy_2-biph** is again unexpected.[1] However, it is worth noting that the Dy−Dy interactions in **Dy_2-biph-crown$_2$** are likely stronger than those in **Dy_2-biph** because of shorter metal−metal distances; thus, by ferromagnetic coupling of two Kramers dysprosium ions, an integer spin is obtained as the spin ground state for **Dy_2-biph-**

DOI: 10.1021/ic5029788
Inorg. Chem. 2015, 54, 2374−2382

crown$_2$. This subsequently increases the QTM and disappearance of the SMM behavior.

In contrast, **Er$_2$-biph** and **Er$_2$-biph-crown$_2$** display similar ac magnetic relaxation dynamics. Under zero applied dc field, both complexes display a tail in the out-of-phase (χ'') susceptibility (Figures S18 and S19 in the SI) at high frequency. Such behavior precludes zero-field SMM behavior in these complexes. Under a 900 Oe applied dc field, both **Er$_2$-biph** and **Er$_2$-biph-crown$_2$** display multiple relaxation dynamics (Figures 4 and S20 and S21 in the SI). At high frequency, **Er$_2$-biph** displays full frequency-dependent peaks with peak maxima shifting toward lower temperatures, indicating slow magnetic relaxation. A secondary peak is also evident at low temperature and frequency, where peak maxima are frequency-independent, indicating QTM. Similarly, **Er$_2$-biph-crown$_2$** also displays full frequency-dependent peaks, indicating a thermal relaxation process as well as a secondary shoulder at low frequency consistent with a secondary QTM relaxation process. In both **Er$_2$-biph** and **Er$_2$-biph-crown$_2$**, the anisotropic barrier was extracted from the frequency-dependent peaks, yielding U_{eff} = 16 K, $\tau_0 = 3.4 \times 10^{-5}$ s and U_{eff} = 25 K, $\tau_0 = 4.7 \times 10^{-6}$ s, respectively (Figures S22 and S23 in the SI).

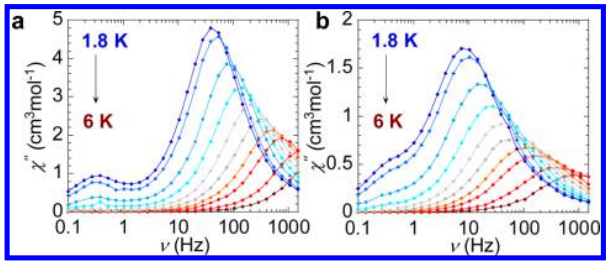

Figure 4. Out-of-phase (χ'') ac magnetic susceptibility for **Er$_2$-biph** (a) and **Er$_2$-biph-crown$_2$** (b) from 1.8−6 K under an applied dc field of 900 Oe.

Ab Initio Calculations. Ab initio calculations were employed in order to acquire more insight into the electronic and magnetic structures and the origin of the magnetic blocking of the investigated compounds. All calculations were performed with the *MOLCAS* program package[28] and were of the CASSCF/RASSI/SINGLE_ANISO type[29] (for computational results and details, see the SI). This computational approach has been successfully applied previously for the investigation of lanthanide compounds.[30−32] In particular, this computational methodology proved reliable in the determination of the orientation of the local magnetic axes in the lowest electronic states of metal sites,[33] and, quite recently, it was proven to give also a trustworthy spectrum of the crystal-field splitting of the lowest J manifolds of lanthanide-based complexes.[34]

Current ab initio calculations are not suitable for treating several magnetic centers at a time. Therefore, suitable fragmentation was imposed. Fragmentation, in our approach, does not imply "deleting atoms from the molecular structure" but rather consists only of replacement of neighboring magnetic sites by their diamagnetic equivalent. In the present case, lutetium(3+) was used in place of neighboring dysprosium(3+) or erbium(3+) sites. All iron(II) sites were kept as they are in all calculations because of their low-spin structure. In all cases, the experimental X-ray structure was used for all calculations without further optimization of the atom positions by computational means. All atoms were described by ANO-RCC relativistic basis sets[35] available in the *MOLCAS* package.[28] The active space of the CASSCF method included all electrons from the last shell spanning seven 4f orbitals. All spin states arising from this active space were optimized, and all (for erbium) or some (for dysprosium) of them were further mixed by spin−orbit interaction in the *RASSI* program. On the basis of the resulting spin−orbit multiplets, the magnetic properties of individual lanthanide sites (i.e., main magnetic axes) were evaluated. Table 2 shows the obtained low-lying energy spectrum of individual lanthanide sites for all investigated compounds in the largest computational model employed. We noticed that the total crystal-field splitting of the ground-state $J = {}^{15}/_{2}$ manifold for **Dy$_2$-biph** and **Dy$_2$-biph-crown$_2$** is almost twice as large as that of **Er$_2$-biph** and **Er$_2$-biph-crown$_2$**. This sharp difference is attributed to the different nature of the ground-state $J = {}^{15}/_{2}$ manifold of Er^{3+} and Dy^{3+} ions, in particular reflected in different Stevens parameters α, β, and γ corresponding to the crystal-field operators O_2, O_4, and O_6.[36] The splitting between the ground- and first excited-state Kramers doublets is about 90 cm^{-1} for **Dy$_2$-biph** and about 51 cm^{-1} for **Dy$_2$-biph-crown$_2$**. We also noticed the much stronger magnetic axiality for the former compound, reflected in the $g_{X,Y}$ values: for the latter compound, they are nearly 1 order of magnitude larger than those in the former one. Because of the lack of symmetry in **Er$_2$-biph**, erbium sites are chemically and electronically different. This is reflected in the obtained energy spectrum of individual erbium sites and in their magnetic axiality. Figure 5 shows the ab initio calculated main magnetic axes and orientation of the local magnetic moments in the ground state with respect to the molecular frames for **Dy$_2$-biph** and **Dy$_2$-biph-crown$_2$**. The magnetic axes of **Er$_2$-biph** and **Er$_2$-biph-crown$_2$** are shown in the SI (Figures S24 and S25).

We note that the magnetic axiality is higher for the erbium site, which has a larger energy gap between the ground- and first excited-state Kramers doublets. For **Er$_2$-biph-crown$_2$**, ab initio calculations revealed a relatively small energy gap between the ground- and first excited-state doublets and a relatively low magnetic axiality. Interestingly, the main anisotropy axis of both **Dy$_2$-biph** and **Dy$_2$-biph-crown$_2$** makes a small angle with the shortest chemical bond of the corresponding dysprosium site, while the main anisotropy axes

Table 2. Energies of the Low-Lying Doublet States Arising from the Splitting of the Ground-State $J = {}^{15}/_{2}$ of Individual Lanthanide Sites in the Investigated Compounds (cm^{-1})

			Er$_2$-biph		
	Dy$_2$-biph	Dy$_2$-biph-crown$_2$	Er1	Er2	Er$_2$-biph-crown$_2$
1	0.0	0.0	0.0	0.0	0.0
2	90.4	50.8	57.9	87.3	22.0
3	233.4	191.1	158.7	174.2	163.7
4	383.4	330.0	194.8	200.9	181.9
5	550.6	506.6	217.1	222.5	201.7
6	750.3	718.9	296.0	323.9	276.3
7	920.9	873.0	470.8	497.4	460.0
8	979.5	942.6	536.4	549.1	510.8
	g Tensors of the Ground-State Kramers Doublet				
g_X	0.038	0.269	0.185	0.081	0.331
g_Y	0.088	0.841	0.401	0.142	0.973
g_Z	19.279	18.934	17.435	17.590	16.946
	Angle of the g_Z Axis with the Shortest Ln−N Chemical Bond (deg)				
	8.48	11.35	84.67	85.99	87.22

DOI: 10.1021/ic5029788
Inorg. Chem. 2015, 54, 2374−2382

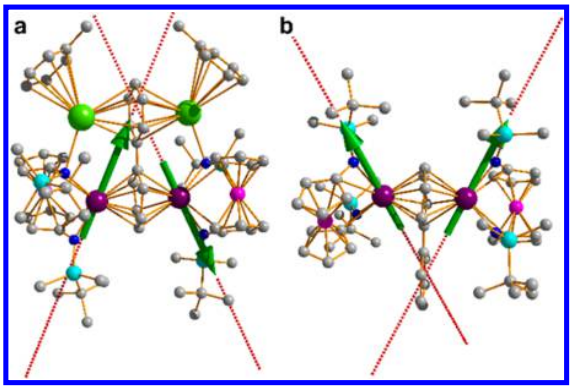

Figure 5. Ab initio calculated main magnetic axes (dashed lines) and orientation of the local magnetic moments in the ground state for **Dy_2-biph** (a) and **Dy_2-biph-crown$_2$** (b) with respect to the molecular frame. Color scheme: Dy, purple; Fe, pink; K, light green; Si, cyan; C, gray; N, blue. Hydrogen atoms are not shown for clarity.

of **Er_2-biph** and **Er_2-biph-crown$_2$** are almost perpendicular to the shortest Er−N chemical bond. This is due to the opposite signs of the Stevens parameters α and β for the ground-state $J = {}^{15}/_{2}$ of dysprosium(3+) and erbium(3+) ions: for the same crystal-field parameters, the splitting effect arising from second- and fourth-rank parameters is opposite.[36] For the investigated compounds, the nitrogen atoms hold a relatively large electrostatic charge (computed Mulliken charges vary from −0.55 to −0.70), which, corroborated with the short distance, induces strong electrostatic and covalent effects, resulting in the largest perturbation to the corresponding lanthanide site. Because this perturbation induces the orientation of the main magnetic axis for the ground-state doublet along the Dy−N chemical bond for dysprosium sites, the magnetic axis of the Kramers doublet that is "destabilized" the most, i.e., the eighth doublet in Table 2, is lying almost perpendicularly to the shortest Dy−N chemical bond. Consequently, because of the opposite signs of the Stevens parameters α and β for the ground-state manifold $J = {}^{15}/_{2}$ of dysprosium(3+) and erbium(3+), for erbium compounds, this perturbation will stabilize the ground-state Kramers doublet, holding the perpendicular orientation of the main magnetic axis to the shortest chemical bond (Table 2). A similar, opposite effect of the almost-identical crystal field on the magnetic anisotropy of erbium and dysprosium ions was recently found for the $[Er(COT)_2]^-$ single-ion magnet.[30]

The obtained ab initio results for individual metal sites were further used for computation of the exchange spectrum and magnetic properties of the binuclear complexes using the *POLY_ANISO* program.[29,37] The exchange interaction between lanthanide sites is considered within the Lines model[38] (for more details, see the SI), while the contribution of the intramolecular dipole−dipole magnetic coupling is accounted for exactly because all of the necessary data are available from the ab initio calculations. Best-fitting Lines parameters of the exchange interaction for the investigated compounds are given in Table 3. On the basis of the resulting exchange spectrum of the entire system, all macroscopic magnetic properties were computed.

The magnetic interaction (exchange + dipolar) between the lowest Kramers doublets on sites can be cast in a good approximation by the noncollinear Ising Hamiltonian:

Table 3. Exchange and Dipolar Interactions (Entering Equation 1) and the Corresponding Low-Lying Exchange Spectrum of Dy_2-biph and Dy_2-biph-crown$_2$ (cm^{-1})

interaction	Dy_2-biph	Dy_2-biph-crown$_2$
dipolar[a]	−2.482	−2.504
exchange	1.056	7.253
Low-Lying Exchange Spectrum of the Binuclear Compounds		
	0.000000	0.000000
	0.000021	0.021005
	0.767187	1.996495
	0.767212	2.024025
	90.716751	49.607745
	90.717581	49.648058
	90.819442	50.385569
	90.822345	50.412137
	90.928407	53.342034
	90.931136	53.371755
	91.044514	54.086462
	91.045231	54.099730
	...	...
g_Z Values in the Two Low-Lying Exchange Doublet States[b]		
	15.531	33.107
	35.315	18.411

[a]Only the term ($\sim z_1 z_2$) of the dipolar interaction is shown here. All terms were included in the *POLY_ANISO* calculation. [b]$g_{X,Y} = 0$ for non-Kramers doublets, in view of the Griffith theorem.[39]

$$\hat{H}_{exch} = -J\hat{S}_{z_1}\hat{S}_{z_2} \quad (1)$$

where $J = J_{dipolar} + J_{exchange}$ is the parameter of the total magnetic interaction between metal sites and $\hat{S}_{z_i} = {}^{1}/_{2}$ is the pseudospin of the ground-state doublet of the corresponding dysprosium and erbium sites.

From Table 3, we noticed that the dipolar coupling in **Dy_2-biph** and **Dy_2-biph-crown$_2$** is antiferromagnetic and of rather similar strength, while the exchange coupling is ferromagnetic and much stronger in the latter compound. While in **Dy_2-biph** the exchange interaction is weaker than the dipolar one, in **Dy_2-biph-crown$_2$**, the situation is opposite. The reason for the sharp discrepancy in the exchange coupling of **Dy_2-biph** compared to **Dy_2-biph-crown$_2$** could be the presence of the two K^+ ions in the former compound that attract a significant amount of electronic density from the C_8 ring, promoting the interaction between lanthanide sites. While inner- versus outer-sphere differences have been previously observed for exchange coupling,[40] a switch from antiferromagnetic to ferromagnetic coupling has not been previously reported. The magnetism computed using the parameters reported in Table 3 compares relatively well with the measured values (Figures 6 and S8 and S9 in the SI).

The insight offered by ab initio calculations allows for rationalization of the SMM behavior of the investigated compounds. Thus, the only compound showing peaks in the out-of-phase ac susceptibility in the absence of an applied static magnetic field is **Dy_2-biph** (Figure S14 in the SI), which has the highest on-site magnetic axiality (Table 2). For **Dy_2-biph-crown$_2$**, only weak peaks are observed in the presence of a static applied magnetic field, suppressing the QTM, which is in line with much larger values of $g_{X,Y}$ in the ground-state Kramers doublet of individual dysprosium ions. This is also true for both erbium complexes, which also show large values of $g_{X,Y}$ in the ground-state doublets (Table 2).

DOI: 10.1021/ic5029788
Inorg. Chem. 2015, 54, 2374−2382

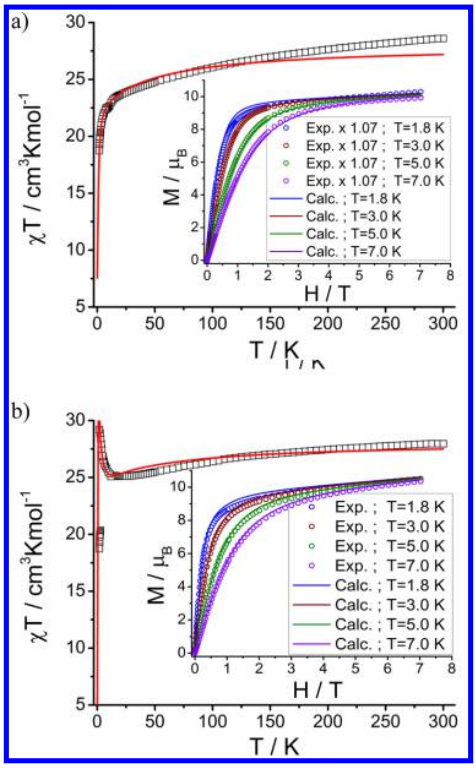

Figure 6. Comparison between the measured (empty figures) and ab initio calculated (lines) magnetic susceptibility and molar magnetization (insets) for **Dy_2-biph** (a) and **Dy_2-biph-crown$_2$** (b).

CONCLUSIONS

We synthesized a series of inverse sandwich dysprosium, erbium, and gadolinium biphenyl complexes with and without potassium coordinated to the neighboring phenyl ring by manipulating the molecules bound to potassium. The nature of the magnetic coupling between the lanthanide ions was surprisingly different: a ferromagnetic interaction was observed in **Dy_2-biph-crown$_2$**, **Er_2-biph**, and **Er_2-biph-crown$_2$**, each having Ln−Ln distances shorter than those of **Gd_2-biph**, **Gd_2-biph-crown$_2$**, and **Dy_2-biph**, for which antiferromagnetic coupling was observed. SMM behavior was observed in **Dy_2-biph** under zero dc field with an energy barrier of 34 K. This barrier significantly increased to 53 K with the application of a 900 Oe dc field, which suppressed QTM. For **Dy_2-biph**, the relaxation barrier primarily arises from the single-ion anisotropy of the dysprosium(III) ion. However, when dysprosium(III) and erbium(III) ions are coupled ferromagnetically, the observed barriers are reduced due to significant QTM because ferromagnetic coupling of the two half-integer spins leads to an integer ground-state spin molecule. Nonetheless, it was remarkable to observe that the secondary coordination environment drastically affects the nature of the magnetic interaction in the two dysprosium systems and, subsequently, the magnet-like behavior shown by the slow relaxation of magnetization.

ASSOCIATED CONTENT

Supporting Information

X-ray crystallographic data in CIF format and X-ray crystallography, magnetic, and ab initio calculation. This material is available free of charge via the Internet at http://pubs.acs.org.

AUTHOR INFORMATION

Corresponding Authors

*E-mail: liviu.ungur@chem.kuleuven.be.
*E-mail: m.murugesu@uottawa.ca.
*E-mail: pld@chem.ucla.edu.

Present Address

‡W.H.: Department of Chemistry, Massachusetts Institute of Technology, Cambridge, MA 02139.

Author Contributions

∥The first two authors contributed equally.

Notes

The authors declare no competing financial interest.

ACKNOWLEDGMENTS

The synthetic work was supported by the NSF (CAREER Grants 0847735 and 1362999 to P.L.D. and Grant CHE-1048804 for NMR spectroscopy). W.H. and P.L.D. thank the Kaner group (UCLA) for a generous gift of KC_8. M.M. thanks the University of Ottawa, NSERC (Discovery and RTI grants), and CFI for their financial support. L.U. is a postdoctoral fellow of the Fonds Wetenschappelijk Onderzoek-Vlaanderen and also gratefully acknowledges INPAC and Methusalem grants of KU Leuven.

REFERENCES

(1) Rinehart, J. D.; Long, J. R. *Chem. Sci.* **2011**, *2*, 2078−2085.
(2) Woodruff, D. N.; Winpenny, R. E. P.; Layfield, R. A. *Chem. Rev.* **2013**, *113*, 5110−5148.
(3) Layfield, R. A. *Organometallics* **2014**, *33*, 1084−1099.
(4) Sorace, L.; Benelli, C.; Gatteschi, D. *Chem. Soc. Rev.* **2011**, *40*, 3092−3104.
(5) Chilton, N. F.; Collison, D.; McInnes, E. J. L.; Winpenny, R. E. P.; Soncini, A. *Nat. Commun.* **2013**, *4*, 2551.
(6) Rinehart, J. D.; Fang, M.; Evans, W. J.; Long, J. R. *J. Am. Chem. Soc.* **2011**, *133*, 14236−14239.
(7) Rinehart, J. D.; Fang, M.; Evans, W. J.; Long, J. R. *Nat. Chem.* **2011**, *3*, 538−542.
(8) Mills, D. P.; Moro, F.; McMaster, J.; van Slageren, J.; Lewis, W.; Blake, A. J.; Liddle, S. T. *Nat. Chem.* **2011**, *3*, 454−460.
(9) Huang, W.; Dulong, F.; Wu, T.; Khan, S. I.; Miller, J. T.; Cantat, T.; Diaconescu, P. L. *Nat. Commun.* **2013**, *4*, 1448.
(10) Diaconescu, P. L.; Arnold, P. L.; Baker, T. A.; Mindiola, D. J.; Cummins, C. C. *J. Am. Chem. Soc.* **2000**, *122*, 6108−6109.
(11) Evans, W. J.; Kozimor, S. A.; Ziller, J. W.; Kaltsoyannis, N. *J. Am. Chem. Soc.* **2004**, *126*, 14533−14547.
(12) Monreal, M. J.; Khan, S. I.; Kiplinger, J. L.; Diaconescu, P. L. *Chem. Commun.* **2011**, *47*, 9119−9121.
(13) Patel, D.; Moro, F.; McMaster, J.; Lewis, W.; Blake, A. J.; Liddle, S. T. *Angew. Chem., Int. Ed.* **2011**, *50*, 10388−10392.
(14) Arnold, P. L.; Mansell, S. M.; Maron, L.; McKay, D. *Nat. Chem.* **2012**, *4*, 668−674.
(15) Diaconescu, P. L.; Cummins, C. C. *Inorg. Chem.* **2012**, *51*, 2902−2916.
(16) Vlaisavljevich, B.; Diaconescu, P. L.; Lukens, W. L.; Gagliardi, L.; Cummins, C. C. *Organometallics* **2013**, *32*, 1341−1352.
(17) Patel, D.; Tuna, F.; McInnes, E. J. L.; McMaster, J.; Lewis, W.; Blake, A. J.; Liddle, S. T. *Dalton Trans.* **2013**, *42*, 5224−5227.
(18) Camp, C.; Mougel, V.; Pécaut, J.; Maron, L.; Mazzanti, M. *Chem.—Eur. J.* **2013**, *19*, 17528−17540.
(19) Pangborn, A. B.; Giardello, M. A.; Grubbs, R. H.; Rosen, R. K.; Timmers, F. J. *Organometallics* **1996**, *15*, 1518−1520.

DOI: 10.1021/ic5029788
Inorg. Chem. 2015, 54, 2374−2382

(20) Bailey, P. J.; Coxall, R. A.; Dick, C. M.; Fabre, S.; Henderson, L. C.; Herber, C.; Liddle, S. T.; Lorono-Gonzalez, D.; Parkin, A.; Parsons, S. *Chem.—Eur. J.* **2003**, *9*, 4820−4828.
(21) Monreal, M. J.; Carver, C. T.; Diaconescu, P. L. *Inorg. Chem.* **2007**, *46*, 7226−7228.
(22) Huang, W.; Upton, B. M.; Khan, S. I.; Diaconescu, P. L. *Organometallics* **2013**, *32*, 1379−1386.
(23) Meyer, G.; Garcia, E.; Corbett, J. D. The Ammonium Chloride Route to Anhydrous Rare Earth Chlorides—The Example of YCl_3. In *Inorganic Syntheses*; John Wiley & Sons, Inc.: New York, 2007; pp 146−150.
(24) Le Roy, J. J.; Jeletic, M.; Gorelsky, S. I.; Korobkov, I.; Ungur, L.; Chibotaru, L. F.; Murugesu, M. *J. Am. Chem. Soc.* **2013**, *135*, 3502−3510.
(25) Shannon, R. *Acta Crystallogr., Sect. A* **1976**, *32*, 751−767; see also http://abulafia.mt.ic.ac.uk/shannon/.
(26) Cucinotta, G.; Perfetti, M.; Luzon, J.; Etienne, M.; Car, P.-E.; Caneschi, A.; Calvez, G.; Bernot, K.; Sessoli, R. *Angew. Chem., Int. Ed.* **2012**, *51*, 1606−1610.
(27) Ishikawa, N.; Iino, T.; Kaizu, Y. *J. Am. Chem. Soc.* **2002**, *124*, 11440−11447.
(28) Aquilante, F.; Vico, L. D.; Ferre, N.; Ghigo, G.; Malmqvist, P. A.; Neograd y, P.; Pedersen, T. B.; Pitonak, M.; Reiher, M.; Roos, B. O.; Serrano-Andres, L.; Urban, M.; Veryazov, V.; Lindh, R. *J. Comput. Chem.* **2010**, *31*, 224−247.
(29) Chibotaru, L. F.; Ungur, L. J. *Chem. Phys.* **2012**, *137*, 064112.
(30) Ungur, L.; Roy, J. J. L.; Korobkov, I.; Murugesu, M.; Chibotaru, L. F. *Angew. Chem., Int. Ed.* **2014**, *53*, 4413−4417.
(31) Ungur, L.; Chibotaru, L. F. *Phys. Chem. Chem. Phys.* **2011**, *13*, 20086−20090.
(32) Chibotaru, L. F.; Ungur, L.; Aronica, C.; Elmoll, H.; Pilet, G.; Luneau, D. *J. Am. Chem. Soc.* **2008**, *130*, 12445−12455.
(33) Ungur, L.; Heuvel, W. V. d.; Chibotaru, L. F. *New J. Chem.* **2009**, *33*, 1224−1230.
(34) Marx, R.; Moro, F.; Dörfel, M.; Ungur, L.; Waters, M.; Jiang, S. D.; Orlita, M.; Taylor, J.; Frey, W.; Chibotaru, L. F.; Slageren, J. v. *Chem. Sci.* **2014**, *5*, 3287−3293.
(35) Roos, B. O.; Veryazov, V.; Widmark, P.-O. *Theor. Chem. Acc.* **2004**, *111*, 345.
(36) Abragam, A.; Bleaney, B. *EPR of Transition Ions*; Oxford University Press: Oxford, U.K., 1970; Table 20.
(37) Ungur, L.; Thewissen, M.; Costes, J.-P.; Wernsdorfer, W.; Chibotaru, L. F. *Inorg. Chem.* **2013**, *52*, 6328−6337.
(38) Lines, M. E. *J. Chem. Phys.* **1971**, *55*, 2977−2984.
(39) Griffith, J. S. *Phys. Rev.* **1963**, *132*, 316−319.
(40) Meihaus, K. R.; Corbey, J. F.; Fang, M.; Ziller, J. W.; Long, J. R.; Evans, W. J. *Inorg. Chem.* **2014**, *53*, 3099−3107.

DOI: 10.1021/ic5029788
Inorg. Chem. 2015, 54, 2374−2382